RSC Applied Polymers

ROYAL SOCIETY OF CHEMISTRY

PAPER

View Article Online
View Journal | View Issue

Open Access Article. Published on 07 April 2025. Downloaded on 12/13/2025 9:58:47 AM.
This article is licensed under a Creative Commons Attribution-NonCommercial 3.0 Unported Licence.

Check for updates

Cite this: *RSC Appl. Polym.*, 2025, **3**, 829

Rheokinetics of ε-caprolactam anionic-ring polymerization applied to the rapid production of thermoplastic composites†

Karima Ben Hamou,[a] Ralf Brüning,[b] Gabriel La Plante,[c] Marie-Hélène Thibault,[a] Jacques Robichaud[a] and Yahia Djaoued *[a]

The present study focuses on the synthesis and structural analysis of poly-ε-caproamide (PA6), produced through anionic polymerization of ε-caprolactam in bulk, utilizing mono and bifunctional activators. The research investigates the physical properties of PA6 synthesized under various polymerization conditions, aiming to understand how these conditions influence the polymer's behavior. The polymerization kinetics were monitored *via* dynamic rheology, offering insights into the progression of ε-caprolactam's conversion into PA6. Microstructural changes in the PA6 samples, including variations in the degree of crystallinity and the formation of α and γ crystalline structures, were systematically studied. These transformations were dependent on both the type and concentration of the activator used, as well as the specific polymerization parameters applied. The interplay between these factors significantly impacted the resulting chemical and physical structure of the PA6 samples. In the latter part of the study, hybrid composites were fabricated by reinforcing poly-ε-caproamide with two distinct types of fiber fabrics by reactive processing, achieving a 25% weight fraction of reinforcement. Scanning electron microscopy (SEM) revealed excellent interfacial adhesion between the fibers and the polymer matrix, confirming the effectiveness of the fabrication process and the potential of these composites for advanced material applications.

Received 21st January 2025,
Accepted 7th April 2025

DOI: 10.1039/d5lp00015g

rsc.li/rscapplpolym

Introduction

Key sustainable green chemical process parameters include solvent-free reactions, quantitative conversion without by-products, and minimal energy consumption. The industrial method of bulk anionic ring-opening polymerization (AROP) of lactams aligns well with these principles, offering an environmentally friendly and cost-effective approach for polyamide synthesis. This method generates no by-products and achieves near-quantitative yields.[1–9] While anionic polymerization of lactams is not a new research area, it has gathered renewed interest in recent years due to its increasing relevance in advanced technological applications. Examples of these applications include reactive vacuum infusion,[10–13] reactive pultrusion,[14–16] reactive resin transfer moulding,[17–19] and reactive rotational moulding.[20–22] Recent reviews highlight advancements in lactam ring-opening polymerization, particularly in catalysis and kinetics, which open new pathways for innovation in this field.[2,23] This research aims to continue the development of poly-ε-caproamide (PA6) by the anionic polymerization of ε-caprolactam. The purpose is to provide an efficient and economical technology that facilitates reactive processing, particularly for thermoplastic composites. In this study, the homopolymerization of ε-caprolactam was initiated using *N*,*N*-dicyclohexylcarbodiimide (DCCI) or *N*-acetylcaprolactam (ACL) as activators, with dicaprolactamato-bis-(2-methoxyethoxo)-aluminate (DL) serving as the catalyst. Despite numerous studies on anionic lactam polymerization since Joyce and Ritter's seminal work in 1941,[24] this specific combination of activators and catalyst had not been explored previously. The present study investigates the impact of various processing parameters on the polymerization kinetics of caprolactam. Key factors include polymerization temperature, catalyst/activator combinations, and concentrations. The primary focus is understanding the rheological behaviour of the anionically initiated ring-opening polymerization of caprolactam, where PA6 is synthesized. These rheological characteristics are crucial as they define the polymers' end properties. This research represents a concerted effort to optimize

[a]*Laboratoire de Recherche en Matériaux et Micro-spectroscopies Raman et FTIR, Université de Moncton – Campus de Shippagan, Shippagan, NB, Canada E8S 1P6. E-mail: yahia.djaoued@umoncton.ca*
[b]*Physics Department, Mount Allison University, Sackville, NB, Canada E4L1E6*
[c]*Faculté d'ingénierie, Université de Moncton – Campus de Moncton, Moncton, NB, Canada E1A 3E9*

† Electronic supplementary information (ESI) available. See DOI: https://doi.org/10.1039/d5lp00015g

© 2025 The Author(s). Published by the Royal Society of Chemistry

Open Access Article. Published on 07 April 2025. Downloaded on 12/13/2025 9:58:47 AM.
This article is licensed under a Creative Commons Attribution-NonCommercial 3.0 Unported Licence.

Table 1 Performed tests

DL/ACL				DL/DCCI			
Sample designation	Catalyst[a] (%)	Activator[a] (%)	Temperature (°C)	Sample designation	Catalyst[a] (%)	Activator[a] (%)	Temperature (°C)
T140-DL/ACL-1.5	1.5	1.5	140	T140-DL/DCCI-0.75	1.5	0.75	140
T160-DL/ACL-1.5	1.5	1.5	160	T160-DL/DCCI-0.75	1.5	0.75	160
T170-DL/ACL-1.5	1.5	1.5	170	T170-DL/DCCI-0.75	1.5	0.75	170
T140-DL/ACL-3	3	3	140	T140-DL/DCCI-1.5	3	1.5	140
T160-DL/ACL-3	3	3	160	T160-DL/DCCI-1.5	3	1.5	160
T170-DL/ACL-3	3	3	170	T170-DL/DCCI-1.5	3	1.5	170

[a] (mol% per 1 mol caprolactam).

bulk polymerization conditions and establish a simple yet robust polymerization technique suitable for reactive moulding operations. By refining this process, the work aims to provide a more practical and scalable solution for industrial applications of PA6, with potential implications for developing advanced thermoplastic composites.

Experimental

Materials

The monomer used in this work was ε-caprolactam (ε-CL) (99%) purchased from TCI AMERICA. The material was dried at 60 °C for 24 h. The catalyst sodium dicaprolactamato-bis-(2-methoxyethoxo)-aluminate (DL) (82 wt% in toluene) was acquired from Katchem, Czech Republic, and used without further treatment. As polymerization activators, *N*-acetylcaprolactam (ACL) (99%) as monofunctional activator have been bought from Alfa Aesar and *N*,*N*-dicyclohexylcarbodiimide (DCCI) (95%) as bifunctional activator was purchased from Thermo Fisher Scientific Chemicals, Inc. Methanol, and sulfuric acid (98%), were purchased from Millipore Sigma. All products were used without further purification.

Two types of fibers were used to produce the hybrid composite samples: Hexcel HexForce 7781 E-glass 8-Harness Satin fabric (299 g m^{-2}), manufactured by Hexcel Corporation (Stamford, CT) and generously supplied by Innov (Shippagan, New Brunswick, Canada), and hemp fibers (*Cannabis sativa* L.) provided by GEMS Consultants Inc. (New Brunswick, Canada). The hemp fibers had an average length of 7 ± 0.5 cm and a diameter of 25 ± 5 μm. To enhance their properties, the hemp fibers underwent a chemical treatment using a 2 wt% aqueous NaOH solution at room temperature.[25] They were immersed in the NaOH solution for 24 hours and then thoroughly washed with distilled water to remove any excess alkali. Acetic acid was applied to neutralize the residual sodium hydroxide.[26] Both sodium hydroxide and acetic acid, used during the treatment, were procured from Millipore Sigma with a purity of 99%.

Polymerization runs

At room temperature, an amount of ε-CL in white granules was melted in a double-necked flask at 100–110 °C. The required amount of catalyst (DL) was added under a nitrogen atmosphere to keep moisture and oxygen out. Because the catalyst concentration significantly impacts the polymer's solidification time, the weight of the compound was carefully controlled. When the temperature reached 140 °C ≤ T_{poly} ≤ 170 °C, the activator (ACL or DCCI) was added to the above mixture to form the polymer. The polymerization reaction began as soon as the activator was injected into the mixture, and after a period, the viscosity rose rapidly, and the solid PA6 was formed. Various formulations were explored, labeled as TX-Catalyst/Activator-Y, where X represents the polymerization temperature, and Y indicates the activator concentration. The catalyst is DL, while the activator is ACL or DCCI. A summary of the formulations examined is provided in Table 1.

Manufacturing of the hybrid composites

A hybrid composite was prepared using 1.5 mol% of a monofunctional activator (ACL) and 1.5 mol% of a DL catalyst at 170 °C. The premix was made at 100–110 °C following the detailed protocol described in the Polymerization Runs section. The experimental design incorporated two types of fibers: glass fibers (GF) and alkali-treated hemp fibers (tHF). The filler content was set at 25 wt% for all composite laminate samples. The hybrid glass/treated hemp fiber composites were produced *via* compression molding in a rectangular steel mold using a hydraulic hot-plate press (Wabash Genesis Model G100-18, Wabash, IN). After homogenization, the premix was quickly transferred into a preheated rectangular mold (190 × 190 × 5 mm), which was then positioned horizontally between the plates of the hot press heated to 170 °C. The composite was cured for 60 minutes under a pressure of 10 tons. Once the polymerization was complete, the mold was cooled, and the composite was removed. Fig. S1† illustrates the flowchart of the fabrication process of the hybrid glass/treated hemp fiber composite samples. Besides the matrix, each composite sample contained a total of five layers with varying glass-to-treated hemp fiber weight fraction ratios of 0 : 25, 10 : 15, 15 : 10, 20 : 5, and 25 : 0.

Analysis methods

FTIR Spectra analyses were performed by Agilent Cary 630 FTIR operated in Attenuated Total Reflection mode. A total of 32 scans were performed to obtain the spectrum within the

 © 2025 The Author(s). Published by the Royal Society of Chemistry

Open Access Article. Published on 07 April 2025. Downloaded on 12/13/2025 9:58:47 AM.
This article is licensed under a Creative Commons Attribution-NonCommercial 3.0 Unported Licence.

wavelength range of 4000 to 400 cm^{-1}, with a resolution of 4 cm^{-1}.

The degree of conversion (DC) of the synthesized samples was determined for various resin formulations at several temperatures. The polymerized samples were ground, weighed to determine the initial mass m_i, and refluxed overnight in methanol. After drying, the final mass m_f was obtained. While the caprolactam monomer dissolves easily in methanol, its polyamide does not, and the degree of conversion was determined according to eqn (1):[27]

$$DC = \frac{m_f}{m_i} \times 100\% \quad (1)$$

Differential Scanning Calorimeter (DSC) measurements were conducted using a TA Q200 V24.11 Build 124 thermal analyzer (New Castle, DE, USA) to determine the melting, glass transition, and crystallization temperatures T_m, T_g, and T_c, respectively. The temperature was scanned from −20 to 300 °C at a heating rate of 10 °C min^{-1} with the sample in a nitrogen atmosphere. The degree of crystallinity (χ_c^{DSC}) was calculated according to eqn (2):

$$\chi_c^{DSC} = \frac{\Delta H_m}{\Delta H_{100}^{\circ}} \times 100\%, \quad (2)$$

where ΔH_{100}° is the melting enthalpy of fully crystalline poly-ε-caproamide (PA6) (190 J g^{-1}),[28] and ΔH_m is it's heat of fusion.

Thermogravimetric analysis (TGA) was performed on a TA Q500 V20.13 Build 39 thermal analysis instrument (New Castle, DE, USA) under a nitrogen atmosphere at a 10 °C min^{-1} heating rate from room temperature up to 700 °C.

Following the procedure outlined in reference,[29] an approximation of the viscosity average molar mass ($\bar{M}_v$) for each sample was obtained by employing diluted solution viscometry with a suspended-level Ubbelohde viscometer maintained at 25 °C in aqueous H_2SO_4 (98%) at a concentration of 0.2 g dl^{-1}. The molar mass of PA6 was determined using the Mark–Houwink equation.[10,30,31] $K = 4 \times 10^{-3}$ dl g^{-1} and $\alpha = 0.7$ are the relevant parameters in this context.[32] The average flow times were calculated from five separate runs.

To know the evolution of the viscosity of the reactive systems according to the reaction time in isothermal mode. Viscosities were measured dynamically at various temperatures on a stress-controlled rheometer DHR (Discovery Hybrid Rheometer, TA Instruments, USA). The premix was quickly introduced into the preheated parallel plate geometry (θ = 25 mm) at the polymerization temperature. The variations in complex viscosity during the polymerization step were then monitored by time sweep oscillatory experiments under a strain amplitude of 10% and an angular frequency of 100 rad s^{-1}. The rheometer chamber was purged with nitrogen for one hour, preventing thermal oxidation and polymerization inhibition and ensuring that the moisture level in the chamber was kept to a minimum. Before introducing a sample, the instrument was first equilibrated at the desired temperature, and the gap was set.

X-ray diffraction (XRD) was carried out with a custom-built θ–θ diffractometer equipped with a pyrolytic graphite monochromator and analyzer crystals. Cu-Kα radiation with wavelength λ = 0.154 nm was used for the measurements. The crystallinity (χ_c^{XRD}) was calculated according to:

$$\chi_c^{XRD} = \frac{A_c}{A_c + A_a} \times 100\%, \quad (3)$$

where A_c is the area under the crystalline curve and A_a is the area under the amorphous curve.

Results and discussion

Chemical features of anionic ring-opening ε-caprolactam polymerization

The anionic ring-opening polymerization process has a complicated chemical mechanism.[33–35] Reversible and irreversible processes consume and regenerate the active species during the anionic ring-opening polymerization of ε-caprolactam.[36] Several side reactions have been reported during polymerization, especially at elevated temperatures.[22,36] The reaction strategy for the anionic ring-opening polymerization of caprolactam is presented in Fig. 1. Two transacylation processes, initiation and propagation, are pivotal in the reaction mechanism of ring-opening polymerization of ε-caprolactam. Initiation occurs when the activator and catalyst engage in an addition, a crucial step that sets the reaction in motion. Repetition of addition and hydrogen abstraction reactions leads to propagation, a process that builds the polymer chain. These processes, along with deactivation, branching, and reversible transacylation, contribute to the formation of yield-side reaction products, heterogeneities in the final polymer structure, and a broad molecular weight distribution.[36] The intricate interplay of the activator and catalyst in these processes underscores the complexity of polymerization.

Impact of activator type and concentration on polymerization rate, monomer conversion, and molecular weight

Anionic polymerization of ε-caprolactam involves a series of exothermic reactions (polymerization) and processes (crystallization). The exothermic nature of polymerization can be used to determine the polymerization rate. Polymerization data are listed in Table 2, where the polymerization time, degree of conversion (DC), and the viscosity average molar mass ($\bar{M}_v$) are given as functions of both the chosen activator and the initial reaction temperature ranged between 140 °C and 170 °C. In this study, both mono and bifunctional activators, *N*-acetylcaprolactam and *N*,*N*′-dicyclohexylcarbodiimide ([A]), were analyzed and the amount of the catalyst [C] ranged from 1.5 to 3 mol%. The amount of activator [A] was chosen to satisfy the following relation, [C] = [A] × *N*, where *N* is the functionality of the activator.

As mentioned above, the reaction consists of three basic steps: (1) dissociation of the catalyst or anion formation, (2) complex formation between the catalyst and the activator, and (3) polymerization through the anions, during which an anion

Open Access Article. Published on 07 April 2025. Downloaded on 12/13/2025 9:58:47 AM.
This article is licensed under a Creative Commons Attribution-NonCommercial 3.0 Unported Licence.

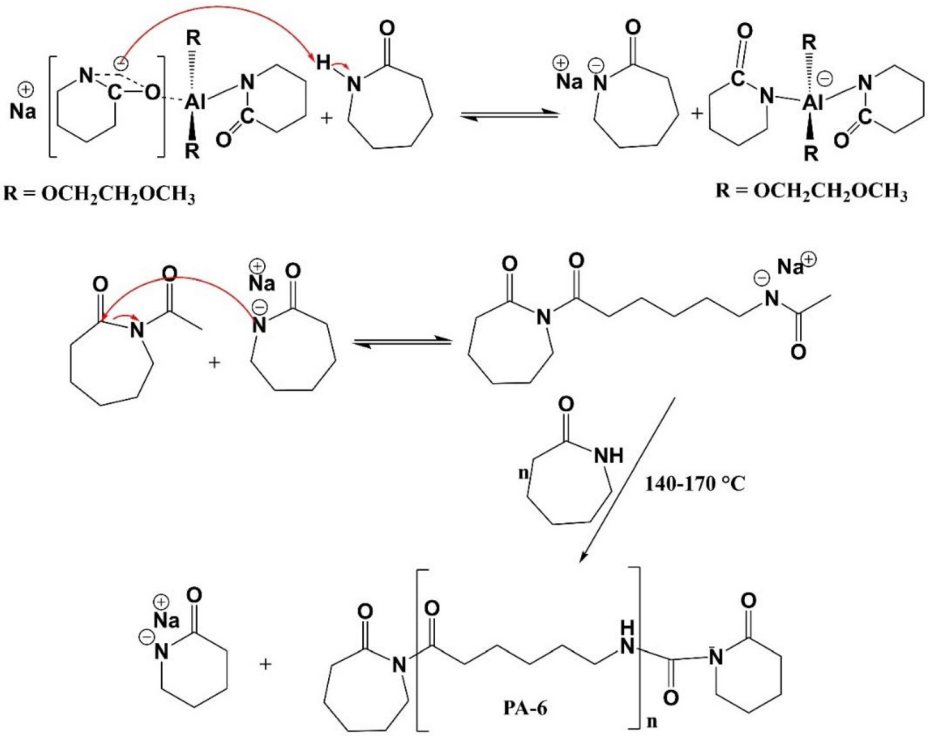

Fig. 1 Illustration of the initiation and propagation steps in the anionic ring-opening polymerization (AROP) of lactams using N-acyllactam as an activator.

Table 2 The impact of activator type and concentration on polymerization rate, degree of conversion, and the viscosity average molar mass

Sample designation	Polymerization time (min)	DC (%)	$\bar{M}_v$ (g mol^{-1})
T140-DL/ACL-1.5	10	97	24 287
T140-DL/ACL-3	6	96	27 171
T160-DL/ACL-1.5	7	99	44 509
T160-DL/ACL-3	1.5	95	31 344
T170-DL/ACL-1.5	3	98	45 223
T170-DL/ACL-3	0.75	95	31 647
T140-DL/DCCI-0.75	40	99	41 036
T140-DL/DCCI-1.5	16	97	27 171
T160-DL/DCCI-0.75	13	99	70 381
T160-DL/DCCI-1.5	4	98	35 394
T170-DL/DCCI-0.75	7	99	76 892
T170-DL/DCCI-1.5	3	98	37 926

is regenerated after every monomer addition.[37] The combination of activator and catalyst primarily determines the reaction rate but is also controlled by the initial polymerization temperature, which will be highlighted in detail in the following section. Fig. S2† shows the change in temperature for two catalyst-activator combinations polymerized at initial temperatures ranging from 140–170 °C. Compared to the bifunctional activator, the polymerization time for complete conversion with the monofunctional activator was very impressive. This is because the DL/DCCI combination does not immediately form a complex, which explains the slow linear conversion increase at the start of the reaction. The carbamoylcaprolactam group is replaced with an acetylcaprolactam group following a single monomer addition. As a result of this group's ability to form a complex with the catalyst, the reaction rate increases over time (after 40 min for T140-DL/DCCI-0.75 and 16 min for T140-DL/DCCI-1.5). The monomer is consumed faster as the catalyst concentration increases because more anions are released, and complexes can form. More activators mean more chain growth in start locations. Thus, Fig. S2† shows that the time needed to consume all monomers up to the equilibrium conversion level decreases, whereas Table 2 shows that the final degree of conversion decreases. Because each catalyst molecule contributes a cation (see Fig. 1), a caprolactam anion must neutralize its positive charge. As the concentration of the catalyst increases, more anions are liberated, and more complexes can form; as a result, the monomer is consumed more quickly. Increasing the amount of activator increases the number of chain growth initiation points. Therefore, the time necessary to consume all monomers up to the equilibrium conversion level lowers, as seen in Fig. S2,† while the final degree of conversion drops, as indicated in Table 2. Each catalyst molecule introduces a cation (see Fig. 1), whose positive charge must be neutralized by a caprolactam anion throughout the reaction. Not all caprolactam polymerizes to compensate for these cations, limiting the highest degree of conversion possible. Increasing the activator concentration increases the proportion

 © 2025 The Author(s). Published by the Royal Society of Chemistry

Open Access Article. Published on 07 April 2025. Downloaded on 12/13/2025 9:58:47 AM.
This article is licensed under a Creative Commons Attribution-NonCommercial 3.0 Unported Licence.

of oligomers with low molecular weight in the final polymer.[38] Being soluble in methanol, these oligomers decrease the conversion rate as assessed by the previously stated approach. Table 2 demonstrates that the measured conversion decreases as the activator and catalyst concentrations increase, and the activator's functionality notably affects the final conversion of the reacted polymers. For the best results, the bifunctional activator (DCCI), should be used to maintain a high and nearly constant degree of conversion. In contrast, the monofunctional activator exhibits a noticeable drop in conversion. But in absolute terms, these conditions result in higher monomer conversion of polycaprolactam compared to conventional methods of ε-caprolactam polymerization.[39]

According to Table 2, the viscosity average molar mass ($\bar{M}_v$) decreases with increasing activator (*i.e.*, catalyst) concentration in the presence of both monofunctional and bifunctional activator in the polymerization mixture. For a given catalyst concentration, the $\bar{M}_v$ of the sample obtained with a monofunctional activator is significantly less than in the case of a bifunctional activator. This occurs because branching reactions can produce species with extremely high molecular weights.[37] Although these types of reactions occur for monofunctional and bifunctional activators, branching is enhanced by bifunctional activators.[40] Van Rijswijk *et al.*[10] suggested that using a slower catalyst-activator combination (*i.e.*, a longer time during which branching can take place), can produce a significant degree of branching, even at lower temperatures. The dependence of the degree of branching on the activator concentration and the reaction rate has also been reported by Mateva *et al.*[40]

The impact of initial polymerization temperature on polymerization rate, monomer conversion, molecular weight, and complex viscosity

There are two ways in which the initial polymerization temperature can affect the reaction rate.[30] On the one hand, at high temperatures, it increases the polymerization rate, whereas on the other hand, it decreases the crystallization rate. As seen in Table 2, the polymerization rate reduced as the initial polymerization temperature increased. This occurred because, according to the Arrhenius equation,[37] the reaction rate constant, k, increased as the polymerization temperature increased. This indicates that, as previously observed,[30,37,41] the polymerization rate increased with increasing polymerization temperature, resulting in a shorter polymerization time. As a result of increasing the initial polymerization temperature, the reaction rate and the degree of monomer conversion increased. According to the literature, the amount of residual CL in PA6 depends on the ring-chain equilibrium characteristic of CL at various temperatures.[36] Table 2 shows the effect of the initial polymerization temperature on the $\bar{M}_v$ of the synthesized polymer. The $\bar{M}_v$ has been enhanced by increasing the initial polymerization temperature, as is evident. This trend is consistent with what has been reported in the literature.[10] One possible explanation is the high energy available during polymerization at higher temperatures, which leads to condensation reactions (branching) between polymer chains.[42]

Rheokinetic investigation of the poly-ε-caproamide reactions

The anionic polymerization of lactams is a typical example of the ionic polymerization path in polymer synthesis. Because the reaction path and kinetics of this reaction vary significantly depending on the initial monomers and activators used, it presents fruitful opportunities for analyses of major rheokinetic patterns in these processes. To understand better the time-dependent growth in complex viscosity during the anionic polymerization of ε-caprolactam using DL/DCCI and DL/ACL combinations, here, we present the evolution of the complex viscosity as a function of time for various isothermal conditions over the range of 140–170 °C while rheological measurements are made. Fig. 2 depicts the evolution of the complex viscosity as a function of time under different isothermal conditions for the DL/ACL system. According to the results of the viscosity profiles, the molecular change caused by reaction effects led to notable variations in rheological behaviour. As shown in Fig. 2, under isothermal conditions, the complex viscosity increased dramatically as the reaction progressed. Indeed, the polymerization-induced increase in molecular weight resulted in a higher complex viscosity.

We examined the temperature's impact on the induction time and viscosity behaviour of the DL/ACL system at two concentrations. The data shows that increasing the temperature significantly shortened the induction time. In contrast, when looking at the effect of catalyst/activator concentration across all three temperatures, it was found that the DL/ACL-1.5 composition required about 10 minutes at 140 °C and 3 minutes at 170 °C to reach the maximum viscosity value, while the DL/ACL-3 composition required about 3 minutes at 140 °C and 0.75 minutes at 170 °C. As mentioned above, a higher quantity of activators resulted in a more significant number of chain development initiation locations. Moreover, more anions were liberated with a higher catalyst concentration, and more complexes could form. The acquired results matched those reported in the literature. Fig. 3 illustrates the complex viscosity-time curve for the DL/DCCI system. The time required to achieve the maximum permissible torque on the instrument was varied from about 40 minutes at 140 °C to 7 minutes at 170 °C for the composition DL/DCCI-0.75 and from 20 minutes at 140 °C to 3 minutes at 170 °C for the composition DL/DCCI-1.5. This time is very close to the time required to achieve near-infinite complex viscosity, also known as total solidification.

When the DCCI activator was used, the polymerization seemed to begin slowly. This is evidenced by the viscosity remaining stable for short durations, despite the absence of an initial complex formation.[10] However, after a single monomer addition, the carbamoylcaprolactam group was replaced by an acetylcaprolactam group. Since the latter was able to form a complex with the catalyst, the reaction rate increased after a while. In this regard, it is worth noting that the induction time decreased with increasing polymerization temperature and DL/DCCI concentration. The reaction was also affected by the amount of the reactive species utilized and

Open Access Article. Published on 07 April 2025. Downloaded on 12/13/2025 9:58:47 AM.
This article is licensed under a Creative Commons Attribution-NonCommercial 3.0 Unported Licence.

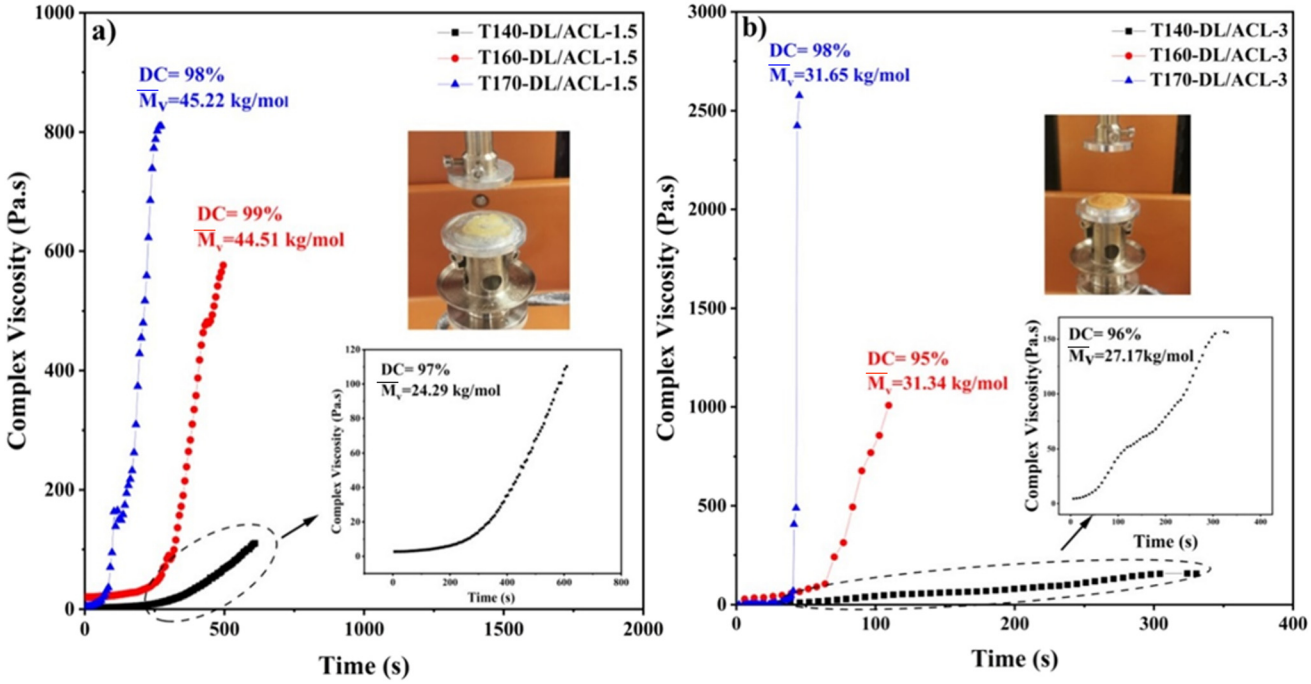

Fig. 2 Isothermal complex viscosity evolution *versus* time during anionic polymerization of ε-caprolactam using DL/ACL as the catalyst/activator system at two concentrations: (a) 1.5/1.5 and (b) 3/3 at 140 °C, 160 °C and 170 °C. The degree of conversion and the molar mass are also shown.

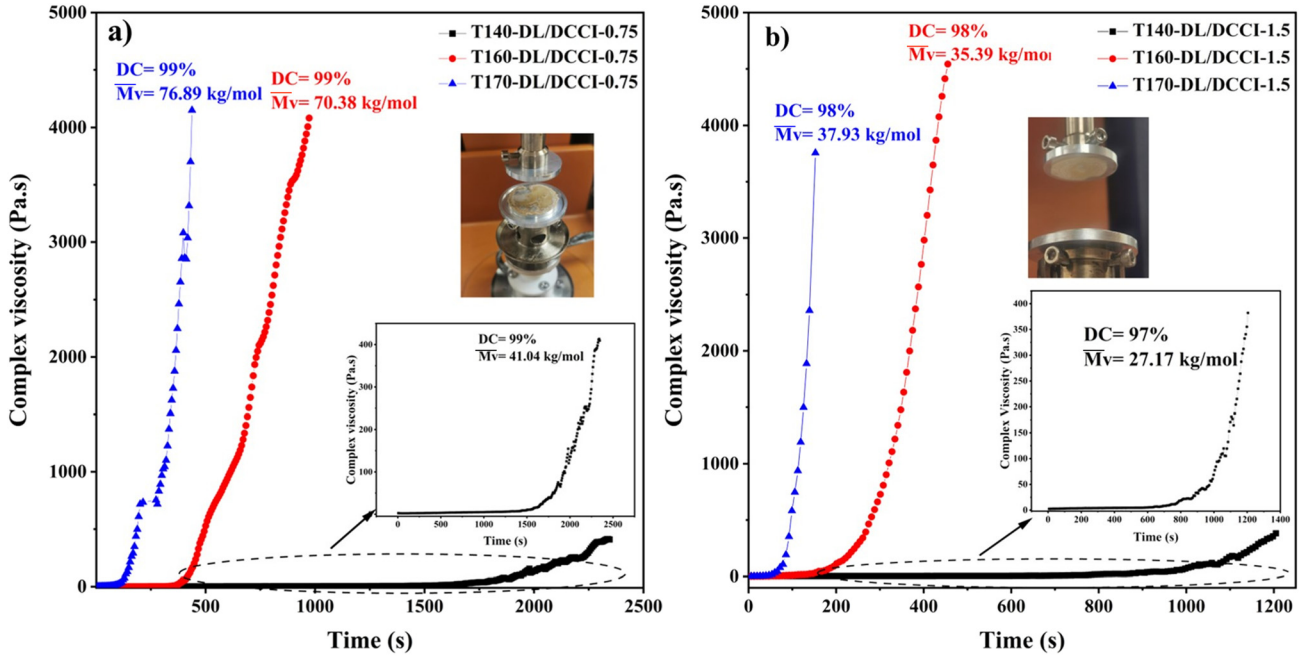

Fig. 3 Isothermal complex viscosity evolution *versus* time during anionic polymerization of ε-caprolactam using DL/DCCI as the catalyst/activator system at two concentrations: (a) 1.5/0.75 and (b) 3/1.5 at 140 °C, 160 °C and 170 °C. The degree of conversion and the molar mass are also shown.

the temperature,[10,22] in addition to the catalyst and activator types. Increasing the polymerization temperature and concentration were demonstrated to boost the polymerization rate.

The results reported so far lead to the conclusion that the combination of DL/ACL led to complex formation, resulting in rapid polymerization and an exponentially increasing viscosity with time. A reduced rate of viscosity increase was seen while using a DL catalyst in combination with DCCI since no complex was formed initially, explaining the slower increase in viscosity. The critical time increase was about 10 minutes for

 © 2025 The Author(s). Published by the Royal Society of Chemistry

Open Access Article. Published on 07 April 2025. Downloaded on 12/13/2025 9:58:47 AM.
This article is licensed under a Creative Commons Attribution-NonCommercial 3.0 Unported Licence.

the DL/ACL system at 140 °C, whereas it was about 40 minutes for the DL/DCCI system at the same temperature. These critical times are calculated using the tangents method when the viscosity grows drastically. The present results also highlight that a higher degree of conversion and molecular weight were obtained with DCCI as the activator. Lastly, this work demonstrates that the reaction time was faster when DL was associated with ACL as the activator.

Thermal properties

Crystallization and melting behaviours of synthesized poly-ε-caproamide. The various thermal events that the samples undergo during the heating process, such as the melting temperature (T_m), the crystallization temperature (T_c), the cold crystallization enthalpy (ΔH_c), as well as the enthalpy of melting or crystallization (ΔH_m) are provided in Table 3.

DL-ACL system. The degree of crystallinity gradually decreases from 56 to 53% for the composition DL/ACL-1.5, and from 52 to 45% for the composition DL/ACL-3 (first heating) by increasing the polymerization temperature from 140 to 170 °C. The first explanation is that the equilibrium degree of crystallinity is lower at higher polymerization temperatures due to the increased thermal motion of the polymer chains. Similarly, it takes longer and longer to reach this equilibrium because the tendency to crystallize decreases as the temperature rises. Another possibility is that branch points disrupt crystal growth, which lowers crystallinity.[43] According to Risch *et al.*[44] findings on cationically polymerized star-branched PA6, the majority of the bulky branch points are concentrated on the surface of the lamellar crystals rather than being integrated into them. As long as no branch point is present, a polymer chain can fold correctly. At that time, a significant alteration to the chain-folding pattern is necessary to include the remaining branches. It is widely accepted that such a disruption will cause the folding process to need more energy, resulting in less order at the lamellar surface. The lamellar thickness often rises at higher crystallization temperatures,[45] which also raises the number of branch points per fold and so intensifies the disrupting impact. On first heating, when increasing the polymerization temperature from 140 to 170 °C, a drop-in polymer melting point of more than 5 °C is observed, as shown in Table 3. Three possible explanations can be given. First of all, Ricco *et al.* have reported that residual caprolactam can lower the polymer melting point.[46] Second, the increasing number of crystal imperfections induced by the formation of branch points can cause a decrease in melting temperatures simply because less energy is required to break down a crystal.[45] It was reported for poly-ε-caproamide (PA6) that branching could even cause a transition in the crystal structure,[39,46] which is the third reason for the decreasing melting points. This will be confirmed by XRD analysis later on. The same conclusions can be drawn from crystal-

Table 3 Thermal data obtained from DSC, TGA and DTG curves of PA6 samples

	DSC data					TGA data			
	Melting process		Crystallization process						
Sample designation	T_m[a] (°C)	ΔH_m[a] (J g^{-1})	χ^c_{DSC}[a] (%)	T_c[a] (°C)	ΔH_c[a] (J g^{-1})	T^d_{onset} (°C)	T^d_{max} (°C)	$T^d_{10\%}$ (°C)	$T^d_{50\%}$ (°C)
T140-DL/ACL-1.5	**221**	**107**	**56**	**185**	**56**	351	422	362	409
	210	69	36	183	65				
T140-DL/ACL-3	**217**	**98**	**52**	**176**	**69**	344	417	357	407
	213	70	37	176	68				
T160-DL/ACL-1.5	**218**	**98**	**52**	**175**	**72**	326	411	336	397
	215	60	32	175	70				
T160-DL/ACL-3	**214**	**88**	**46**	**172**	**72**	320	407	333	396
	211	62	33	172	73				
T170-DL/ACL-1.5	**216**	**100**	**53**	**173**	**70**	353	410	334	400
	214	59	31	172	67				
T170-DL/ACL-3	**212**	**85**	**45**	**170**	**71**	331	405	334	394
	210	59	31	169	67				
T140-DL/DCCI-0.75	**221**	**111**	**58**	**170**	**69**	309	408	324	383
	212	59	31	168	70				
T140-DL/DCCI-1.5	**217**	**99**	**52**	**173**	**70**	269	325	289	322
	211	60	31	168	68				
T160-DL/DCCI-0.75	**217**	**93**	**50**	**176**	**67**	328	432	359	420
	215	56	29	176	67				
T160-DL/DCCI-1.5	**216**	**113**	**59**	**168**	**71**	304	426	321	379
	210	64	34	166	70				
T170-DL/DCCI-0.75	**213**	**95**	**50**	**173**	64	341	457	385	443
	214	55	28	171	63				
T170-DL/DCCI-1.5	**216**	**103**	**54**	**173**	**68**	332	437	348	423
	211	61	32	170	69				

[a] The values in the top and bottom rows correspond to the first and second scans, respectively.

Open Access Article. Published on 07 April 2025. Downloaded on 12/13/2025 9:58:47 AM.
This article is licensed under a Creative Commons Attribution-NonCommercial 3.0 Unported Licence.

linity degree and melting point data from the second heating, which are generally characterized by slightly lower values.

It is also important to note that the second heat traces of all produced samples feature two peaks (as shown in Fig. S3 and S4†). After a second heating, a lower and new peak is seen at the typical melting point. The polymerization of caprolactam at initial temperatures between 140 and 170 °C (*i.e.*, below the melting point of poly-ε-caproamide) may result in a material with a combination of α and g crystalline structures. Puffr *et al.*[36] stated that as many as five melting endotherms may occur in samples of PA6 with the mixed α and g structures: the peaks of original and recrystallized γ structures; the peaks of original and recrystallized α structures (higher by several degrees); and also a small peak approximately 10 °C above crystallization temperature (T_c), assigned to the most defective crystals formed by secondary crystallization. In Fig. S3 and S4,† the two peaks seen on the DSC thermograms, possibly arising from the original α and γ structures formed during polymerization because the sample was not exposed to thermal history for recrystallization.

DL-DCCI system. Table 3 demonstrates that the amount of catalyst and activator used in samples and the initial polymerization temperature affect the melting point and crystallinity degree. The melting point of all produced samples decreased with increased catalyst and activator concentrations. As mentioned above, this phenomenon has been explained by branching reactions that can occur during AROP.[34,37] Rijswijk *et al.*[10] reported that these reactions occur for mono- and bifunctional carbamoylcaprolactam activators, but branching is improved for di-functional activators. The DSC curves of the second run are in Fig. S5 and S6† showed that during the synthesis of poly-ε-caproamide using DL/DCCI combination, two types of crystals could appear: α structure and γ structure.[47] The melting point can be lowered if the α structure content increases due to excessive branching. Table 3 also presents the crystallinity degree of the samples calculated according to eqn (2). The degree of crystallinity gradually decreases from 58 to 50% for the composition DL/DCCI-0.75 (first heating) by increasing the polymerization temperature from 140 to 170 °C. This decrease in crystallinity was related to the rise in molecular weight, indicating that the crystallization of PA6 was complicated by the branching structures produced by the bifunctional activator.[48]

Thermal stability of synthesized poly-ε-caproamide. The thermal stability of the synthesized polymers was studied by thermogravimetric analysis (TGA). The results of the thermogravimetric analysis carried out on various syntheses of poly-ε-caproamide (PA6) are given in Fig. S7 and S8,† along with their first derivative, also known as the derivative thermogravimetric (DTG) curves. They show the variations of the sample's weight loss when heated as a function of the temperature. Moreover, the main degradation characteristics were collected in Table 3. The temperatures T^{d}_{onset}, $T^{d}_{10\%}$, and $T^{d}_{50\%}$, correspond to the onset temperature of degradation, 10% and 50% weight loss, respectively, T^{d}_{max} is the temperature of maximum mass change as noted from the TGA thermograms.

DL-ACL system. As seen in Fig. S7,† the thermal profile revealed that all samples were burned entirely under a nitrogen atmosphere before reaching 500 °C. The onset decomposition temperatures of samples increased with the decrease in catalyst and activator concentrations. This trend indicated that samples with lower concentrations of catalyst and activator were more thermally stable. Derivative thermogravimetric (DTG) plots supported this tendency as well. The maximum weight loss rate at (T^{d}_{max}) was higher for samples with lower catalyst and activator concentrations. As previously reported in TGA thermograms, this finding increases the poly-ε-caproamide (PA6) degradation at an early stage. The T^{d}_{max}, as estimated from DTG curves, is slightly dependent on the polymerization temperature, from one sample to the next, with no discernible relationship to the synthesis conditions.

DL-DCCI system. Fig. S8† shows the TGA thermograms and the corresponding first DTG curves for the formulation DL/DCCI at two concentrations. As estimated from TGA thermograms curves, the onset decomposition temperatures (T^{d}_{onset}), of the samples as well as the temperature of maximum mass change (T^{d}_{max}), are slightly dependent on the concentration of activator and catalyst at different polymerization temperatures. Similar to the case of DL-ACL in the previous section, the thermal stability of the DL-DCCI samples improved when the quantities of the catalyst and activator were reduced. The influence of initial polymerization temperature on the thermal stability of the poly-ε-caproamide (PA6) materials is shown in Table 3. The results in Table 3 indicate that the temperature of initial degradation (T^{d}_{onset}), and the temperature of maximum mass change (T^{d}_{max}) increased with increasing initial polymerization temperature from 140 °C to 170 °C.

Microstructural investigations. It is commonly known that the crystalline phase of polyamides comprises layers of macromolecules with hydrogen bonds. Crystallographically, poly-ε-caproamide (PA6) can be found in two distinct forms: the α-phase and the γ-phase.[49,50] The α-phase is characterized by its monoclinic structure, with hydrogen bonds forming between antiparallel chains. Even though the γ-phase is also monoclinic, it is a metastable compared to the α-form.[51–54] With X-ray diffraction being such a powerful tool, χ_c^{XRD} of all polymerized samples has also been analyzed by WAXS for a more in-depth comparison of the different structures made by the two activators.[45,55]

DL-ACL system. Fig. 4 shows the 1D WAXD diffractograms of poly-ε-caproamide (PA6) utilizing the DL/ACL catalyst/activator combination. Additionally, deconvolution of all WAXD profiles was carried out as indicated previously and Fig. 4c illustrates a representative example.[56,57] The results for total crystallinity, content of α and γ-PA6, and the relation between the two crystalline forms were calculated and tabulated in Table 4. The *d*-spacing (d_{hkl}) of a successive atomic (hkl) plane was calculated with experimentally obtained θ_{hkl} by using Bragg's law:

$$d_{hkl} = \frac{\lambda}{2 \sin \theta_{hkl}}, \quad (4)$$

where λ = 1.54178 Å is the wavelength of Cu Kα X-ray radiation.

According to previous research,[56,58] the two peaks with 2θ at about 20° and 24° were assigned to the (200) and (002/202)

 © 2025 The Author(s). Published by the Royal Society of Chemistry

Open Access Article. Published on 07 April 2025. Downloaded on 12/13/2025 9:58:47 AM.
This article is licensed under a Creative Commons Attribution-NonCommercial 3.0 Unported Licence.

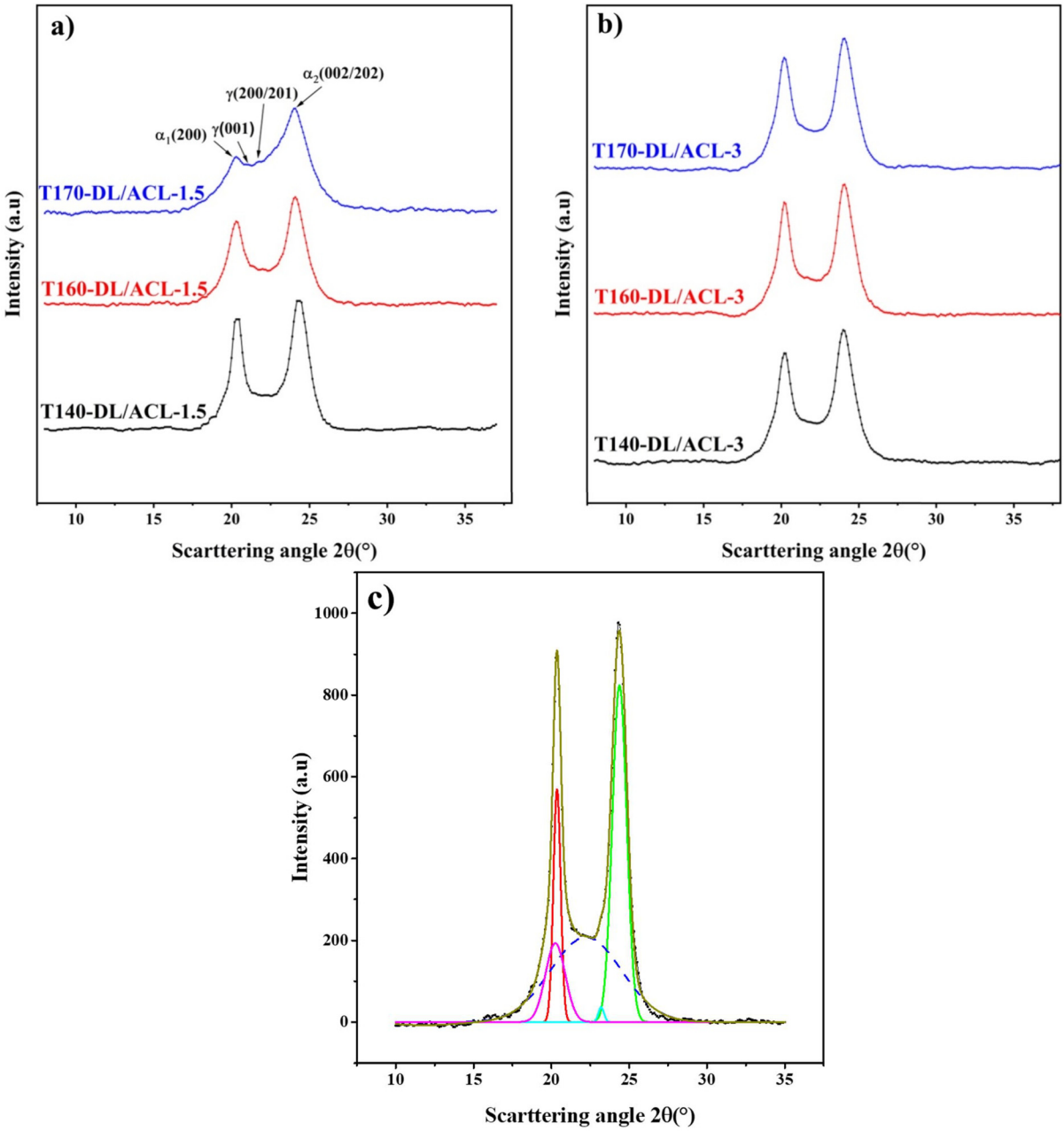

Fig. 4 1D WAXD intensity profiles of the poly-ε-caproamide (PA6) using DL/ACL as the catalyst/activator system at two concentrations, (a) DL/ACL-1.5, (b) DL/ACL-3 at different polymerization temperatures and (c) Selected WAXS pattern of T140-DL/ACL 1.5 sample and its fitting with Gaussian peaks: crystalline peaks are represented by solid lines, while dashed lines represent the amorphous halo.

crystallographic planes of the monoclinic unit cell of the α-PA6 polymorph. Additionally, two Gaussian peaks corresponding to (001) and (200) crystalline planes with 2θ between 22 and 23° were discovered, indicative of the PA6 γ-crystalline form with a pseudo-hexagonal unit cell.

It is well-known that FTIR spectroscopy is one of the most well-established methods for the characterization of nylons and that it provides information about the crystalline phase of polyamide samples.[59,60] Fig. 5 illustrates the FTIR spectra of poly-ε-caproamide (PA6) samples at several polymerization conditions, along with characteristic infrared bands and their roles. The bands at 3196 cm^{-1} and 1654 cm^{-1} in the spectra of the monomer ε-caprolactam correspond to the stretching vibrations of the N–H and C═O bonds, respectively,[61] and are coupled with the self-associated hydrogen bonds produced between C═O and N–H that define the amide II mode. The bands in the 1465–1150 cm^{-1} range correspond to the methyl alkyl group (CH_2) from cyclic lactam related to the bands in the 3500 and 2750 cm^{-1} region. The bands at 1486 and 1438 cm^{-1} correspond to the scissor vibration in the (CH_2)

Open Access Article. Published on 07 April 2025. Downloaded on 12/13/2025 9:58:47 AM.
This article is licensed under a Creative Commons Attribution-NonCommercial 3.0 Unported Licence.

Table 4 Overall crystallinity and polymorph content in synthesized PA samples

Sample designation	Crystallinity Index (%)			α/γ	*d*-Spacing (Å)		ICP (Å)	$\frac{d\alpha_{200}}{d\alpha_{\frac{002}{200}}}$
	α-Phase[a]	γ-Phase[a]	χ^{c}_{XRD} [b]		$\alpha_{1(200)}$	$\alpha_{2(002/202)}$		
T140-DL/ACL-1.5	**46.00**	**11.5**	**57.5**	**4.0**	**4.477**	**3.748**	**0.728**	**0.837**
T140-DL/ACL-3	39.4	12.6	52.0	3.1	4.505	3.799	0.706	0.843
T160-DL/ACL-1.5	**40.2**	**8.9**	**49.1**	**4.5**	**4.492**	**3.790**	**0.702**	**0.844**
T160-DL/ACL-3	35.2	9.3	44.5	3.8	4.507	3.800	0.707	0.843
T170-DL/ACL-1.5	**29.4**	**17.8**	**47.2**	**1.6**	**4.496**	**3.794**	**0.702**	**0.844**
T170-DL/ACL-3	29.6	11.9	41.5	2.5	4.507	3.802	0.705	0.843
T140-DL/DCCI-0.75	**41.5**	**16.7**	**58.2**	**2.4**	**4.464**	**3.748**	**0.715**	**0.840**
T140-DL/DCCI-1.5	25.0	11.0	36.0	2.3	4.453	3.765	0.688	0.845
T160-DL/DCCI-0.75	**32.8**	**16.3**	**49.1**	**2.0**	**4.429**	**3.756**	**0.673**	**0.848**
T160-DL/DCCI-1.5	24.7	6.3	31.0	3.9	4.446	3.794	0.652	0.853
T170-DL/DCCI-0.75	**34.4**	**8.6**	**43.0**	**4.0**	**4.453**	**3.800**	**0.652**	**0.853**
T170-DL/DCCI-1.5	17.7	13.3	31.0	1.3	4.477	3.748	0.728	0.837

[a] $\alpha\text{-Phase}\,(\%) = \frac{A\alpha_c}{A_c + A_a} \times 100$; $g\text{-Phase}\,(\%) = \frac{A\gamma_c}{A_c + A_a} \times 100$. [b] χ^{c}_{XRD} is determined using the deconvolution method (Gaussian fitting with fitting coefficients $r^2 \approx 0.99$).

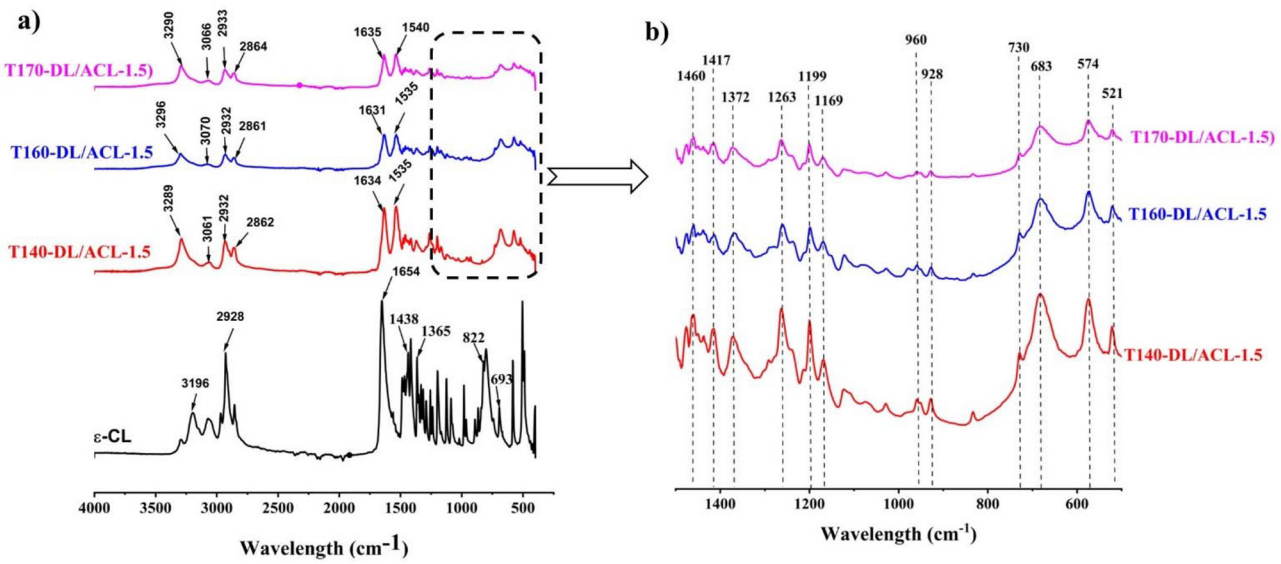

Fig. 5 FTIR spectra of the studied poly-ε-caproamide (PA6) synthesized utilizing a DL/ACL system at varying polymerization temperatures. (a) 4000–400 cm^{-1}, (b) 1500–500 cm^{-1}.

group, whereas the band at 1417 cm^{-1} refers to bending vibrations in the same group. Moreover, the bands at 1365, 1312, 1290, 1258, and 1198 cm^{-1} correspond to the amide group covalently bound to the alkyl group ($NH–CH_2$). The lactam C═O bond was detected at 1654 cm^{-1} and confirmed by the 822 and 693 cm^{-1} bands. However, the spectra of poly-ε-caproamides (PA6) display two bands at 3290 and 1535 cm^{-1}, ascribed to hydrogen bond stretching and bending vibration in amide II, respectively. The 1635 cm^{-1} band is associated with mode I amide bond bending vibrations. Torsion in amide mode I and mode II hydrogen bonds are attributed to the 683 cm^{-1} and 574 cm^{-1} bands, respectively. Also, the presence of two bands at 1199 and 1169 cm^{-1} is according to amide mode III. The carbonyl (C═O) band is located at 1635 cm^{-1} and overlaps with the mode I band of the amide. As previously stated, the (O═CN) bond related to the caprolactam ring was broken (by ring opening) due to the catalyst, and the sodium–caprolactam was formed; this is confirmed since a band is located at 3074 cm^{-1}. In addition, the ring opening is confirmed by the band's presence at 1263 cm^{-1}, which corresponds to the C–N aliphatic bond. Finally, in the poly-ε-caproamides (PA6) CH_2 rocking band area, there are three bands. Sandeman and Keller assigned the 928 cm^{-1} band of the α-form of PA6 to the rocking mode CH_2.[62] Asai *et al.*[63] and Miyake[64] ascribe the remaining two bands at 730 and 683 cm^{-1} to the NH out-of-plane deformation mode (the amide V band). All phases are produced during polymerization, regardless of the raw materials, monomers, and syn-

 © 2025 The Author(s). Published by the Royal Society of Chemistry

Open Access Article. Published on 07 April 2025. Downloaded on 12/13/2025 9:58:47 AM.
This article is licensed under a Creative Commons Attribution-NonCommercial 3.0 Unported Licence.

thesis conditions. In the process of re-crystallization, the γ-phase is eliminated for material exposure. The primary peak in the DSC analysis at around 221–212 °C and the main peaks in the diffraction patterns at 2 = 20° and 24°, as stated previously, indicate that the phase (monoclinic crystal) is the predominant and stable crystalline phase in the synthesized PA6.

The findings of XRD measurements, presented in Table 4, show that the degree of crystallinity of poly-ε-caproamide (PA6) samples decreased as the amount of catalyst/activator increased, in agreement with the degree of crystallinity determined by DSC analysis listed in Table 3. Increasing the catalyst/activator concentration results in an elevation in polymerization temperature because of a rise in polymerization rate (*i.e.*, exothermic polymerization). The temperature at which polymerization occurs affects the process in two different ways. When heated to high temperatures, it has the opposite effect of slowing the crystallization rate and speeding up the polymerization rate.[65] However, the crystallization rate is very high at low temperatures, and reactive groups can become caught inside developing crystals before they can polymerize. This can only happen when the temperature is very low. When polymerization occurs at temperatures higher than 170 °C, the crystallization rate is reduced, although the polymerization rate remains high.[30]

Table 4 illustrates the effect of initial polymerization temperature on the degree of crystallinity of the synthesized polymer. As the initial polymerization temperature rose from 140 °C to 170 °C, the degree of crystallinity diminished. Because of the competitive nature of polymerization and crystallization in this process, the higher thermal motion of the polymer chains, and also the enhanced rate of branching at higher temperatures,[37,46] the reduction in crystallinity of synthesized poly-ε-caproamide (PA6) that can be achieved by increasing the initial temperature of polymerization is caused by a combination of these factors. The fraction of α-PA6 predominates in all poly-ε-caproamide (PA6) samples, with α/γ > 1 for both DL/ACL-1.5 and DL/ACL-3 formulations. The *d*-spacings of α(200), α(002)/(202) of α-PA6 using DL/ACL as the catalyst/activator system at two concentrations and varying polymerization temperatures are shown in Table 4. A crystalline perfection index (ICP) is derived from the relationship between crystalline perfection and crystallinity to quantify variations in crystalline perfection. The index of chain packing (ICP) is defined as the difference of the *d*-spacings for both the (200), (002)/(202) peaks,[66] ICP = $\Delta d = d_{200} - d_{002/202}$.

Fig. 6 demonstrates that the crystal lattice parameters of poly-ε-caproamide (PA6) are impacted by both the catalyst/activator concentration and the polymerization temperature, as indicated by the rise in *d*-spacings with increasing polymerization temperature and catalyst/activator concentration. With increasing catalyst/activator incorporation into the PA6 chain, the resulting changes in crystal lattice properties become statistically significant. This leads to significant morphological alterations and significant disruption of the crystal structure. The Δ*d* of the synthesized poly-ε-caproamide (PA6) is around 0.702–0.728 Å for DL/ACL: 1.5/1.5, and around

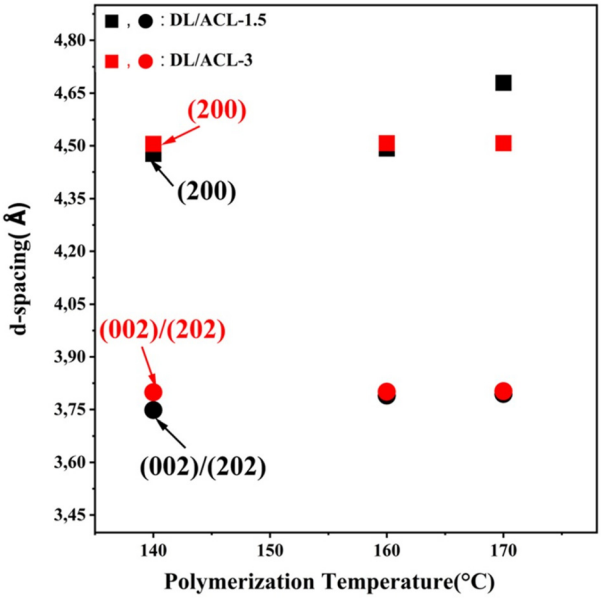

Fig. 6 Change in *d*-spacing of some (*hkl*) diffraction of the studied poly-ε-caproamide (PA6) using DL/ACL as the catalyst/activator system at two concentrations at different polymerization temperatures.

0.705–0.707 Å for DL/ACL: 3/3 depending on the polymerization temperature.

With the DL/ACL-1.5 formulation, T140-DL/ACL-1.5 exhibited ICP = 0.728 Å, which was greater than poly-ε-caproamides synthesized at 160 °C (T160-DL/ACL-1.5) and 170 °C (T170-DL/ACL-1.5). Murthy *et al.*[66] reported that a structure with a higher ICP corresponds to an energetically lower and more stable PA6 lattice. However, when comparing samples of the DL/ACL-3 formulation, we found that the ICP was roughly constant from one to the next, with no clear correlation to the synthesis conditions. Poly-ε-caproamides (PA6) chain packing index does not appear to be affected by polymerization temperature. For the DL/ACL-1.5 formulation, both T160-DL/ACL-1,5 and T170-DL/ACL-1.5 have $da_{200}/da_{002/202}$ of about 0.844, which represents the ratio c/a of unit cell.[67] This is a little bit greater than T140-DL/ACL-1.5 (0.837), and it suggests that the distance between hydrogen-bonded sheets (*i.e.* $d\alpha_{002/202}$) in the unit cell is slightly larger than that of T140-DL/ACL-1.5. A comparison of samples of the DL/AC-3 formulation reveals that the distance between hydrogen-bonded sheets is constant over all three polymerization temperatures, with a $d\alpha_{200}/d\alpha_{002/202}$ ratio of around 0.843.

DL-DCCI system. Fig. 7 shows the 1D WAXD diffractograms of poly-ε-caproamide (PA6) utilizing the DL-DCCI catalyst/activator combination. As illustrated in the figure, the diffraction pattern indicates that two polymorphs of poly-ε-caproamide (PA6) coexist in all materials (α and γ). These are identified by the characteristic peaks at 2θ = 22°, and at 2θ = 23°, associated with the γ phase (pseudo-hexagonal), while the α phase (monoclinic) has the characteristic peaks at 2θ = 20 and 24°.

Open Access Article. Published on 07 April 2025. Downloaded on 12/13/2025 9:58:47 AM.
This article is licensed under a Creative Commons Attribution-NonCommercial 3.0 Unported Licence.

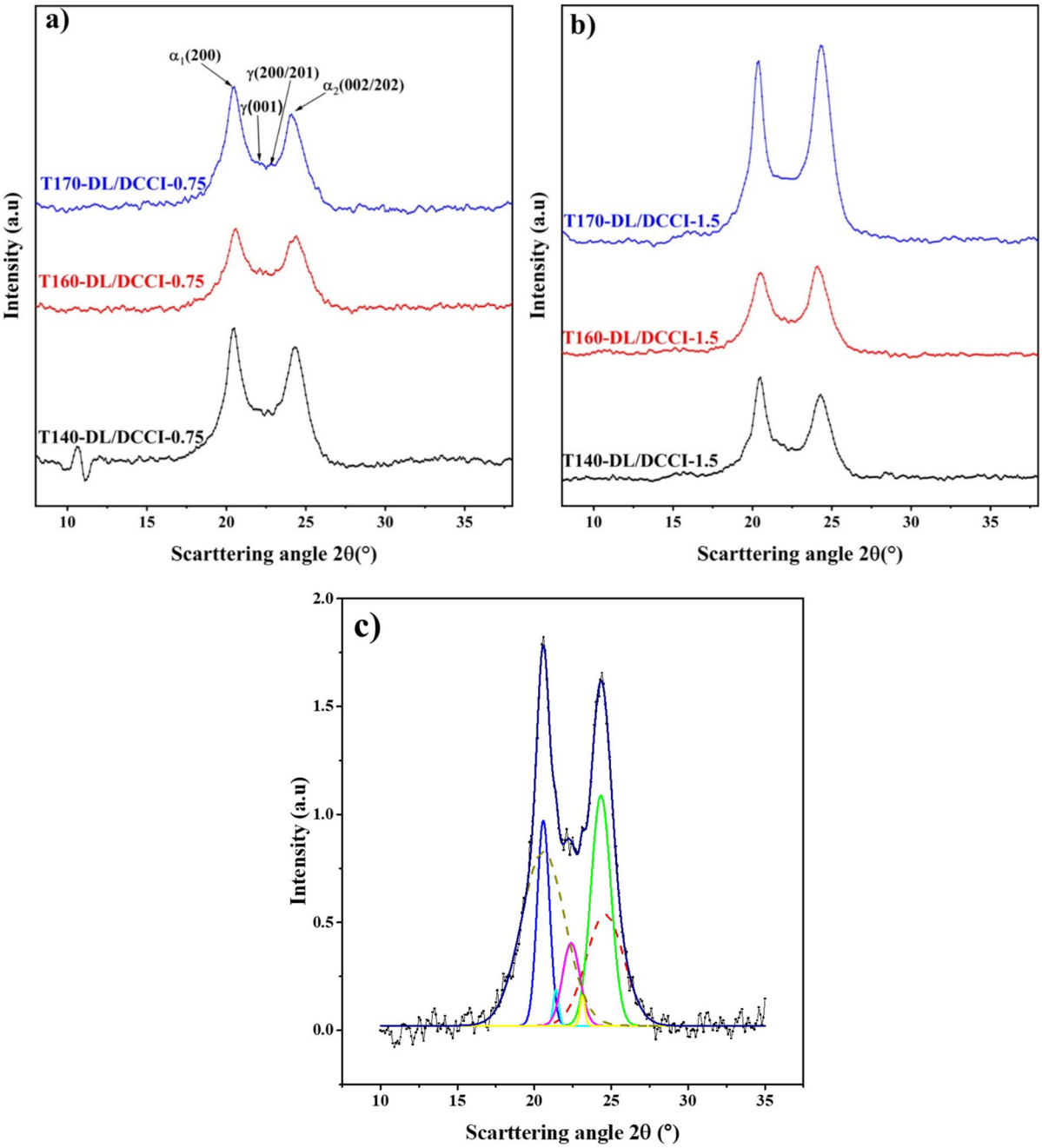

Fig. 7 1D WAXD intensity profiles of the poly-ε-caproamide (PA6) using DL/DCCI as the catalyst/activator system at two concentrations, (a) DL/DCCI-0.75, (b) DL/DCCI-1.5 at different polymerization temperatures and (c) selected WAXS pattern of T160-DL/DCCI-0.75 sample and its fitting with Gaussian peaks: crystalline peaks are represented by solid lines and dashed lines represent the amorphous halo.

This is consistent with the findings of the IR investigation presented below. As seen in Fig. 8. The IR spectrum of the obtained homopolymer presents strong absorption bands at 3290 cm^{-1} (N–H stretch vibration), 1635 cm^{-1} (amide I, C═O), and 1536 cm^{-1} (amide II, N–H deformation) which are characteristic of the amide groups existing in the trans planar conformation. As indicated earlier, the amide II band is extremely sensitive to the crystalline structure corresponding to the α-phase.[59,60] Furthermore, the out-of-plane bends of the NH (amide V) and C═O (amide VI) groups, which appear at 684 and 575 cm^{-1}, respectively, are polymorph sensitive and indicate that the form of the crystalline phase of homopolymer is α-type.[59,60,68] As stated before, the results show that monoclinic crystal is the most common and stable crystalline phase in the synthesized PA6.

Based on the XRD data reported in Table 4, it is clear that the degree of crystallinity of poly-ε-caproamide (PA6) samples is dependent on both the catalyst/activator concentration and

 © 2025 The Author(s). Published by the Royal Society of Chemistry

Open Access Article. Published on 07 April 2025. Downloaded on 12/13/2025 9:58:47 AM.
This article is licensed under a Creative Commons Attribution-NonCommercial 3.0 Unported Licence.

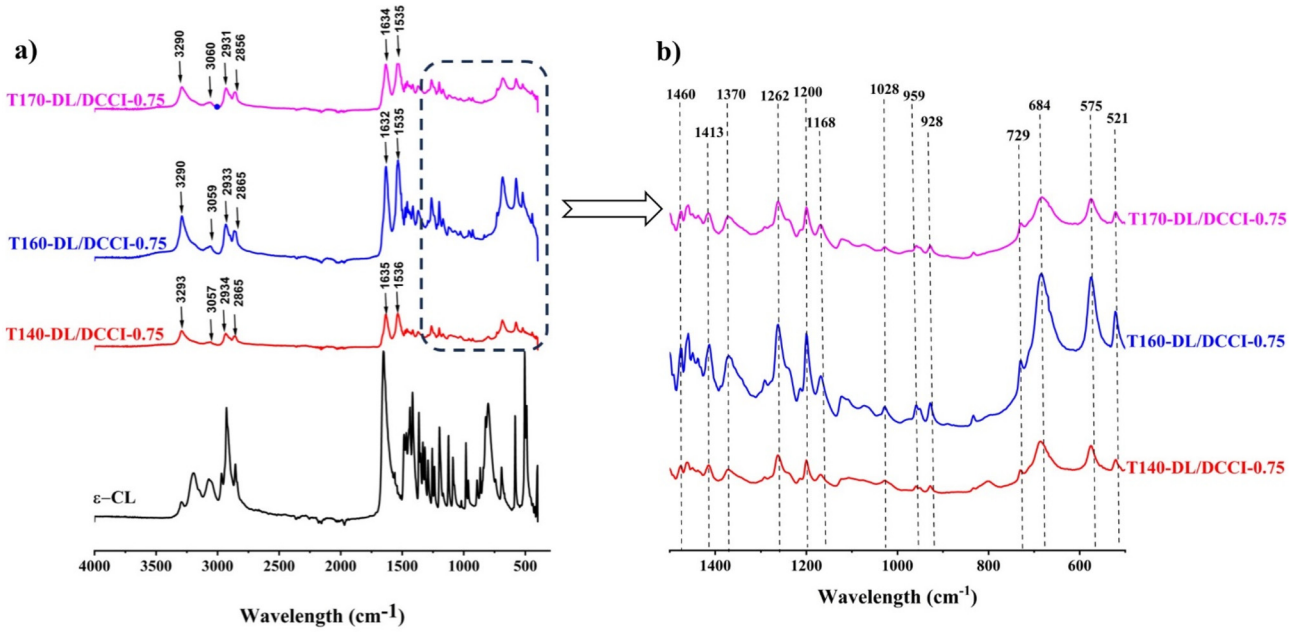

Fig. 8 FTIR spectra of poly-ε-caproamide (PA6) synthesized utilizing a DL-DCCI system at varying polymerization temperatures. (a) 4000–400 cm^{-1}, (b) 1500–500 cm^{-1}.

polymerization temperature. Increasing the amounts of bifunctional activator and catalyst reduced the crystallinity. DSC analysis shows that the degree of crystallinity tends to go the same way. Since the activator *N*,*N*-dicyclohexylcarbodiimide (DCCI) has two functions, two or less acyllactam functions can start the polymerization process. The macromolecular chains cannot reorganize into a perfect crystalline form due to changes in chain length and, most likely, increased chain mobility due to diminished protonic contact between NH and CO groups.

The effect of initial polymerization temperature on the degree of crystallinity of the produced polymer is depicted in Table 4. As shown before for the system DL/ACL, the degree of crystallinity decreased when the initial polymerization temperature increased from 140 °C to 170 °C. Due to the competitive nature of polymerization and crystallization in this process, the higher thermal motion of the polymer chains, and the enhanced rate of branching at higher temperatures,[37,38] increasing the initial temperature of polymerization can reduce the crystallinity of synthesized poly-ε-caproamide (PA6).

The *d*-spacings of α(200), α(002)/(202) and the index of chain packing (ICP) of α-PA6 using DL/DCCI as the catalyst/activator system at two concentrations at varying polymerization temperatures are shown in Table 4.

Fig. 9 demonstrates that the crystal lattice parameters of poly-ε-caproamide (PA6) is impacted by both the catalyst/activator concentration and the polymerization temperature, as indicated by the rise in *d*-spacings with increasing polymerization temperature and catalyst/activator concentration. With increasing catalyst/activator incorporation into the PA6 chain,

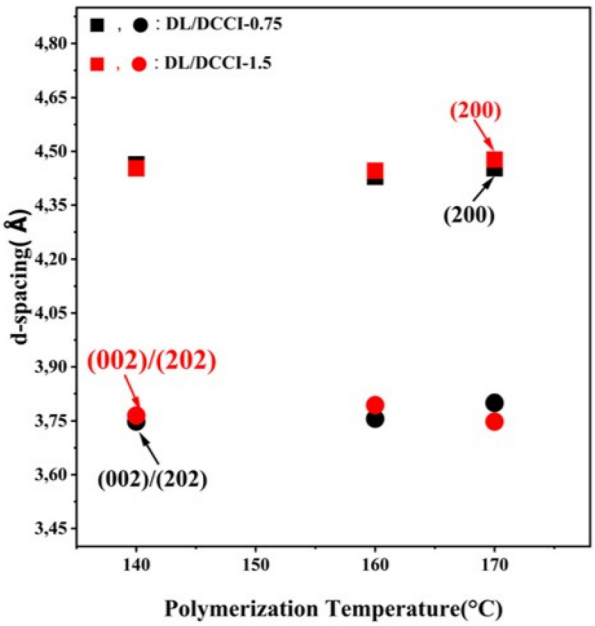

Fig. 9 Change in *d*-spacing of some (*hkl*) diffraction of the studied formulations of poly-ε-caproamide (PA6) using DL/DCCI as the catalyst/activator system at two concentrations at different polymerization temperatures.

the resulting changes in crystal lattice properties become statistically significant. This leads to significant morphological alterations and significant disruption of the crystal structure.

With the DL/DCCI-0.75 formulation, T140-DL/DCCI-0.75 exhibited ICP = 0.715 Å, which was greater than poly-ε-caproa-

Open Access Article. Published on 07 April 2025. Downloaded on 12/13/2025 9:58:47 AM.
This article is licensed under a Creative Commons Attribution-NonCommercial 3.0 Unported Licence.

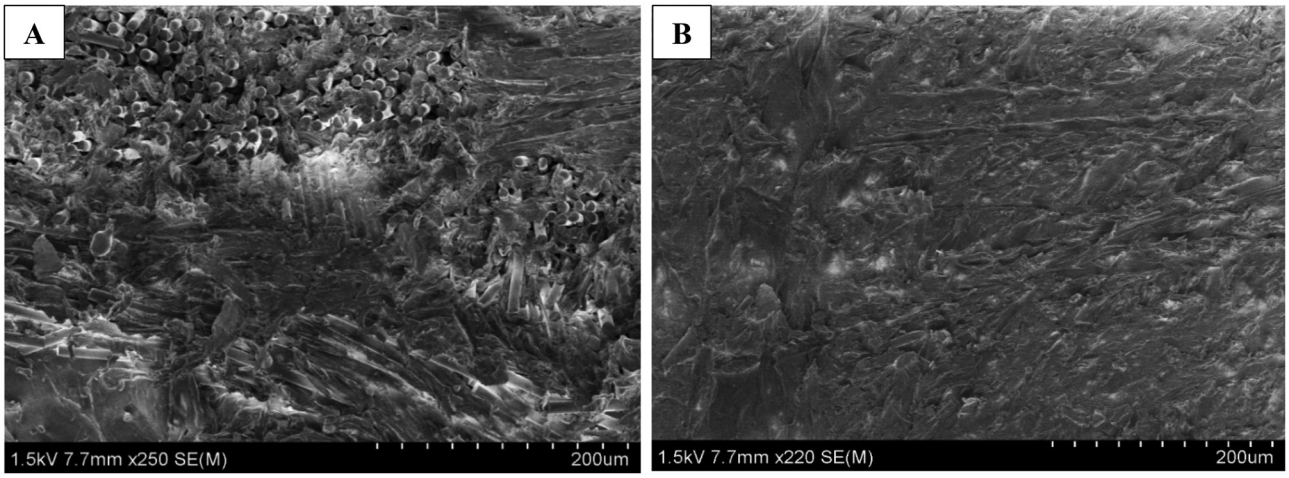

Fig. 10 Cross-sectional SEM images illustrating (A) the edge and (B) the middle sections of a hybrid composite composed of E-glass (20 wt%) and hemp fibre (5 wt%).

mides synthesized at 160 °C (T160-DL/DCCI-0.75) and 170 °C (T170-DL/DCCI-0.75). Comparing samples of the DL/DCCI-1.5 formulation, we noticed that T170-DL/DCCI-1.5 had a higher ICP than T140-DL/DCCI-1.5 and T170-DL/DCCI-0.75. Murthy *et al.*[66] reported that a structure with a higher ICP corresponds to an energetically lower and more stable PA6 lattice.

For the DL/DCCI-0.75 formulation, the $d\alpha_{200}/d\alpha_{002/202}$ ratio, which represents the ratio c/a of unit cell,[67] of T170-DL/DCCI-0.75, it has a ratio of about 0.853. This is a little bit greater than that of T140-DL/DCCI-0.75 and T160-DL/DCCI-0.75 (0.840), and it suggests that the distance between hydrogen-bonded sheets (*i.e.* $d\alpha_{002/202}$) in the unit cell is slightly greater than that of T170-DL/DCCI-0.75. Comparison of samples of the DL/DCCI-1.5 formulation, shows that T160-DL/DCCI-1.5 has a larger distance between hydrogen-bonded sheets with a $d\alpha_{200}/d\alpha_{002/202}$ ratio around 0.853 compared to T140-DL/DCCI-1.5 and T170-DL/DCCI-1.5.

In brief, the effect of the activator on the structure of poly-ε-caproamides (PA6) is governed by two factors: (a) changes in the rate of the polymerization and crystallization process and, (b) changes in the chemical structure due to the incorporation of the activator into the polymer chain.[69] In fact, the reported data suggest that the type of catalyst-activator combination exerts a significant influence on the polymerization and subsequent crystallization of PA6. By varying the amount of appropriately chosen activators, it is possible to control the crystallinity level throughout a wide range. According to the findings of the present experiments, both the type and quantity of activating additives have a substantial impact on the bulk structural development of poly-ε-caproamides (PA6).

Feasibility of using the optimized DL/ACL combination in the compression molding process. Based on the earlier discussion, a 1.5 mol% monofunctional activator (ACL) and a 1.5 mol% DL catalyst were used at a temperature of 170 °C for the preparation of a hybrid composite, utilizing two types of fiber fabrics: treated Hemp fiber and 8-harness satin weave style E-glass fabric. As shown in Fig. S9,† hemp/glass hybrid composites were successfully fabricated using PA6, and the process proceeded without any detectable inhibition of the polymerization reaction. Future studies will further elucidate these details. Fig. 10 presents SEM images of the fracture surfaces from tensile tests, confirming excellent interfacial adhesion between the hemp and glass fibers and the polymer matrix, with no delamination between layers. Additionally, the SEM analysis demonstrated superior fiber wetting and impregnation.

Conclusions

The bulk anionic polymerization of ε-caprolactam was investigated with focus on the influence of two catalyst-activator systems: sodium dicaprolactamato-bis-(2-methoxyethoxo)-aluminate (DL) with *N*-acetylcaprolactam (ACL), and DL with *N*,*N*′-dicyclohexylcarbodiimide (DCCI). The study identifies the polymerization temperature, as well as the type and concentration of the activators, as critical parameters influencing the polymerization dynamics and polymer properties. Increasing the initial polymerization temperature reduces polymerization time and concomitantly decreases crystallinity. However, as the polymerization temperature rises, the average molar mass of the polymer increases. Furthermore, a combination of higher polymerization temperature and lower catalyst-activator concentration yields a higher degree of monomer conversion. On the other hand, higher concentrations of catalyst and activator accelerate polymerization but reduce the average molar mass. A comparative analysis of the catalyst-activator combinations reveals that the DL/ACL system is the most effective for achieving rapid polymerization. Material characterization was performed using DSC, WAXD, and FTIR. These techniques confirm that the α-phase, a monoclinic crystalline structure, is the predominant and thermodynamically stable phase in the synthesized polyamide 6 (PA6). The results underscore the

 © 2025 The Author(s). Published by the Royal Society of Chemistry

Open Access Article. Published on 07 April 2025. Downloaded on 12/13/2025 9:58:47 AM.
This article is licensed under a Creative Commons Attribution-NonCommercial 3.0 Unported Licence.

critical role of processing conditions in tailoring polymer properties and the significance of the DL/ACL system for efficient and controlled polymerization. E-glass/treated hemp fibers hybrid composites using polyamide 6 through anionic polymerization have been fabricated successfully with no observable inhibition of the polymerization process by the presence of these fibers and strong adhesion between the fibers and matrix. Future research will examine the influence of fiber content, processing parameters, and polymerization conditions on these composites' physical, thermomechanical, and microstructural properties.

Author contributions

Karima Ben Hamou: conceptualization, data curation, investigation, methodology, writing – original draft. Ralf Brüning: data curation, investigation, calculation, writing – reviews & editing. Jacques Robichaud: data curation, formal analysis, writing – reviews & editing. Marie-Hélène Thibault: data curation, formal analysis, funding acquisition, writing – reviews & editing. Gabriel LaPlante: data curation, funding acquisition, writing – reviews & editing. Yahia Djaoued: conceptualization, data curation, supervision, project administration, funding acquisition, writing – review & editing.

Data availability

The data supporting this article have been included as part of the ESI.†

The FTIR, DSC, TGA, DTG, XRD, and rheological data supporting this study's findings are provided within the manuscript and ESI.†

Conflicts of interest

There are no conflicts to declare.

Acknowledgements

The financial support from the Atlantic Canada Opportunities Agency (grant #212225), the New Brunswick Innovation Fund (grant # RIF2019-025), the National Sciences and Engineering Research Council (NSERC) of Canada (grant #2023-05942), the Regional Development Corporation of New Brunswick (grant #11266), the John R. Evans Leaders Fund (Canada Foundation for Innovation) (grant #27741), the Mitacs Accelerate (grant #IT16139/FR48699/NB-ISDE).

References

1 S. Russo, S. Maniscalco and L. Ricco, *Polym. Adv. Technol.*, 2015, **26**, 851–854.
2 M. Wilhelm, R. Wendel, M. Aust, P. Rosenberg and F. Henning, *J. Compos. Sci.*, 2020, **4**, 1–19.
3 T. Ageyeva, I. Sibikin and J. Karger-Kocsis, *Polymers*, 2018, **10**, 357.
4 C. W. Choi, J. W. Jin, H. Lee, M. Huh and K. W. Kang, *Fibers Polym.*, 2019, **20**, 1021–1028.
5 J. un Jang, H. S. Lee, J. W. Kim, S. Y. Kim, S. H. Kim, I. Hwang, B. J. Kang and M. K. Kang, *Chem. Eng. J.*, 2019, **373**, 251–258.
6 E. Rusu, *J. Compos. Mater.*, 2020, **54**, 345–362.
7 M. Jiang, H. Tan, L. Jiang, J. Duan, X. Gu, L. Feng and C. Zhang, *Ind. Eng. Chem. Res.*, 2024, **63**, 19476–19485.
8 K. Ben Hamou, R. Bruning, G. LaPlante, M. Thibault, J. Robichaud and Y. Djaoued, *J. Appl. Polym. Sci.*, 2024, **141**, 1–15.
9 Z. Gao, R. Zhao and X. Ning, *Chem. Eng. J.*, 2025, **504**, 158758.
10 K. van Rijswijk, H. E. N. Bersee, A. Beukers, S. J. Picken and A. A. van Geenen, *Polym. Test.*, 2006, **25**, 392–404.
11 K. van Rijswijk, A. A. van Geenen and H. E. N. Bersee, *Composites, Part A*, 2009, **40**, 1033–1043.
12 J. J. E. Teuwen, A. A. Van Geenen and H. E. N. Bersee, *J. Thermoplast. Compos. Mater.*, 2012, **25**, 965–986.
13 S. Kashani Rahimi and J. U. Otaigbe, *Polym. Compos.*, 2019, **40**, 1104–1116.
14 K. van Rijswijk and H. E. N. Bersee, *Composites, Part A*, 2007, **38**, 666–681.
15 S. Epple and C. Bonten, *AIP Conf. Proc.*, 2014, **1593**, 454–457.
16 K. Chen, M. Jia, H. Sun and P. Xue, *Materials*, 2019, **12**, 463.
17 M. Dkier, M. Yousfi, K. Lamnawar and A. Maazouz, *Eur. Polym. J.*, 2019, **120**, 109227.
18 A. Maazouz, K. Lamnawar and M. Dkier, *Composites, Part A*, 2018, **107**, 235–247.
19 Z. Kovács, Á. Pomázi and A. Toldy, *Polym. Degrad. Stab.*, 2022, **195**, 109797.
20 E. Harkin-Jones and R. J. Crawford, *Polym. Eng. Sci.*, 1996, **36**, 615–625.
21 G. H. Rusu, M. Rusu, E. Rusu, A. Stoleriu and C. A. Teaca, *Polym.-Plast. Technol. Eng.*, 2000, **39**, 233–247.
22 N. Barhoumi, A. Maazouz, M. Jaziri and R. Abdelhedi, *eXPRESS Polym. Lett.*, 2013, **7**, 76–87.
23 S. Russo and E. Casazza, *Ring-Opening Polymerization of Cyclic Amides (Lactams)*, Elsevier B.V., 2012, vol. 4.
24 R. M. Joyce and D. M. Ritter *U. S. Pat.* 2251519, 1941.
25 A. Bledzki and J. Gassan, *Prog. Polym. Sci.*, 1999, **24**, 221–274.
26 M. Le Troedec, D. Sedan, C. Peyratout, J. P. Bonnet, A. Smith, R. Guinebretiere, V. Gloaguen and P. Krausz, *Composites, Part A*, 2008, **39**, 514–522.
27 K. van Rijswijk, S. Lindstedt, D. P. N. Vlasveld, H. E. N. Bersee and A. Beukers, *Polym. Test.*, 2006, **25**, 873–887.
28 N. V. Dencheva, J. F. B. Braz and Z. Z. Denchev, *J. Appl. Polym. Sci.*, 2022, **139**, 1–17.

Open Access Article. Published on 07 April 2025. Downloaded on 12/13/2025 9:58:47 AM.
This article is licensed under a Creative Commons Attribution-NonCommercial 3.0 Unported Licence.

29 W.-M. Kulicke, *Viscosimetry of Polymers and Polyelectrolytes*, Springer Science & Business Media, 2004.
30 K. Van Rijswijk, H. E. N. Bersee, W. F. Jager and S. J. Picken, in *Composites Part A: Applied Science and Manufacturing*, Elsevier Ltd, 2006, vol. 37, pp. 949–956.
31 B. Lu, K. Lamnawar, A. Maazouz and H. Zhang, *Soft Matter*, 2016, **12**, 3252–3264.
32 R. Mateva and O. Delev, *Polym. J.*, 1995, **27**, 449–460.
33 R. Puffr and J. Šebenda, *Eur. Polym. J.*, 1972, **8**, 1037–1044.
34 R. S. Davé, R. L. Kruse, L. R. Stebbins and K. Udipi, *Polymer*, 1997, **38**, 939–947.
35 R. Mateva and N. Dencheva, *J. Polym. Sci., Part A: Polym. Chem.*, 1992, **30**, 1449–1462.
36 R. Puffr and V. Kubanek, *Lactam-Based Polyamides*, CRC Press, 1991, vol. I.
37 K. Udipi, R. S. Davé, R. L. Kruse and L. R. Stebbins, *Polymer*, 1997, **38**, 927–938.
38 K. Ueda, M. Hosoda, T. Matsuda and K. Tai, *Polym. J.*, 1997, **30**, 186–191.
39 S. Russo, A. Imperato, A. Mariani and F. Parodi, *Macromol. Chem. Phys.*, 1995, **196**, 3297–3303.
40 R. Mateva, P. Petrov, S. Rousseva, R. Dimitrov and G. Zolova, *Eur. Polym. J.*, 2000, **36**, 813–821.
41 S. Davtyan, H. Zakaryan, A. Tonoyan and G. Varderesyan, *e-Polym.*, 2007, **7**, 1–8.
42 K. J. Kim, D. S. Hong and A. R. Tripathy, *J. Appl. Polym. Sci.*, 1997, **66**, 1195–1207.
43 R. Mateva, O. Delev and E. Kaschcieva, *J. Appl. Polym. Sci.*, 1995, **58**, 2333–2343.
44 B. G. Risch, G. L. Wilkes and J. M. Warakomski, *Polymer*, 1993, **34**, 2330–2343.
45 J. R. Ebdon, *Polym. Int.*, 1992, **27**, 207–208.
46 L. Ricco, S. Russo, G. Orefice and F. Riva, *Macromolecules*, 1999, **32**, 7726–7731.
47 S.-P. Rwei, P. Ranganathan and Y.-H. Lee, *Polymers*, 2019, **11**, 472.
48 C. L. Zhang, L. F. Feng and G. H. Hu, *J. Appl. Polym. Sci.*, 2006, **101**, 1972–1981.
49 D. R. Holmes, C. W. Bunn and D. J. Smith, *J. Polym. Sci.*, 1955, **17**, 159–177.
50 H. Arimoto, M. Ishibashi, M. Hirai and Y. Chatani, *J. Polym. Sci., Part A: Gen. Pap.*, 1965, **3**, 317–326.
51 N. S. Murthy, S. M. Aharoni and A. B. Szollosi, *J. Polym. Sci., Polym. Phys. Ed.*, 1985, **23**, 2549–2565.
52 N. S. Murthy, R. G. Bray, S. T. Correale and R. A. F. Moore, *Polymer*, 1995, **36**, 3863–3873.
53 Y. Liu, L. Cui, F. Guan, Y. Gao, N. E. Hedin, L. Zhu and H. Fong, *Macromolecules*, 2007, **40**, 6283–6290.
54 X. Liu and Q. Wu, *Polymer*, 2002, **43**, 1933–1936.
55 C. A. Taylor, *Acta Crystallogr., Sect. A*, 1970, **26**, 700–701.
56 J. M. Samon, J. M. Schultz and B. S. Hsiao, *Polymer*, 2000, **41**, 2169–2182.
57 N. Dencheva, T. G. Nunes, M. J. Oliveira and Z. Denchev, *J. Polym. Sci., Part B: Polym. Phys.*, 2005, **43**, 3720–3733.
58 N. Dencheva, T. Nunes, M. J. Oliveira and Z. Denchev, *Polymer*, 2005, **46**, 887–901.
59 M. I. Kohan, *Nylon Plastics Handbook*, Hanser, Munich, Germany, 1995.
60 S. M. Aharoni, *n-Nylons: their synthesis, structure, and properties*, 1997.
61 J. C. Farias-Aguilar, M. J. Ramírez-Moreno, L. Téllez-Jurado and H. Balmori-Ramírez, *Mater. Lett.*, 2014, **136**, 388–392.
62 I. Sandeman and A. Keller, *J. Polym. Sci.*, 1956, **19**, 401–435.
63 M. Asai, M. Tsuboi, T. Shimanouchi and S. I. Mizushima, *J. Phys. Chem.*, 1955, **59**, 322–325.
64 A. Miyake, *J. Polym. Sci.*, 1960, **44**, 223–232.
65 R. M. Hedrick, J. D. Gabbert and M. H. Wohl, in *ACS Symposium Series*, 1985, pp. 135–162.
66 N. S. Murthy, H. Minor and R. A. Latif, *J. Macromol. Sci., Part B: Phys.*, 1987, **26**, 427–446.
67 N. S. Murthy, *Polym. Commun.*, 1990, **32**, 301–305.
68 J. L. Yeh, J. F. Kuo and C. Y. Chen, *Mater. Chem. Phys.*, 1994, **37**, 161–169.
69 R. Mateva, O. Delev and S. Rousseva, *Eur. Polym. J.*, 1997, **33**, 1377–1382.

 © 2025 The Author(s). Published by the Royal Society of Chemistry